Electrochimica Acta 213 (2016) 740–751

Contents lists available at ScienceDirect

Electrochimica Acta

journal homepage: www.elsevier.com/locate/electacta

Microstructural and electrochemical analysis of Sb_2O_5 doped-Ti/RuO_2-ZrO_2 to yield active chlorine species for ciprofloxacin degradation

Ricardo E. Palma-Goyes[a], Jorge Vazquez-Arenas[b,*,1], Carlos Ostos[c], Franklin Ferraro[d], Ricardo A. Torres-Palma[a], Ignacio Gonzalez[b]

[a] Grupo de Investigación en Remediación Ambiental y Biocatálisis, Instituto de Química, Facultad de Ciencias Exactas y Naturales, Universidad de Antioquia UdeA, Calle 70 No. 52-21, Medellín, Colombia
[b] Departamento de Química, Universidad Autónoma Metropolitana-Iztapalapa, Av. San Rafael Atlixco No 186, C.P 09340, México D.F, Mexico
[c] Grupo CATALAD, Instituto de Química, Facultad de Ciencias Exactas y Naturales, Universidad de Antioquia UdeA, Calle 70 No. 52-21, Medellín, Colombia
[d] Departamento de Ciencias Básicas, Fundación Universitaria Luis Amigo', Transversal 51A # 67B 90, Medellín, Colombia

ARTICLE INFO

Article history:
Received 24 March 2016
Received in revised form 3 July 2016
Accepted 28 July 2016
Available online 29 July 2016

Keywords:
DSA
RuO_2
ciprofloxacin
active chlorine
degradation mechanism

ABSTRACT

A Sb_2O_5 doped-Ti/RuO_2-ZrO_2 (Ti/SbRuZr) electrode is used to perform the abatement of ciprofloxacin (CIP, $C_{17}H_{18}FN_3O_3$). The catalyst was prepared using the Pechini method, and subsequently characterized by XRD, SEM-EDS, EIS and CV. The microstructural analysis of Ti/SbRuZr shows the formation of RuO_2 (*P4₂/mnm*) and ZrO_2 (*P2/m*) crystalline phases, with an average crystallite size about twice (61.2 nm) lower than Ti/RuO_2 (109 nm). Additionally, SEM micrographs reveal that ZrO_2 affects the morphological features of the deposited RuO_2 layer, turning it into a more heterogeneous material. The electrode capacity was evaluated through the elimination of antibiotic activity (AA) of CIP, revealing that 83 and 45% of AA was removed using Ti/SbRuZr and Ti/RuO_2, respectively at 0.19 A h L^{-1}. According to CV analysis, the electrochemical mechanism for CIP degradation was found to proceed through active chlorine species (Cl_2-active) on Ti/SbRuZr. This facile kinetics occurring on the ternary catalyst resulted from a high charge transfer resistance for oxygen evolution reaction, as revealed by EIS analysis. HPLC, HPLC-MS, and density functional theory were employed to propose a reaction pathway for CIP degradation. Findings from this work stands out prospective applications of anodic electrochemical oxidation to efficiently eliminate CIP, and the associated proliferation of antibiotic resistant microorganisms in aqueous media.

1. Introduction

Fluoroquinolones (FQs) is a class of broad-spectrum antibiotic widely used to treat bacterial agents for human, veterinary and aquaculture applications [1]. Ciprofloxacin is the most prescribed FQ for complicated urinary tract infections, sexually transmitted diseases and skin infections [2], and it can be found in pharmaceutical and hospital wastewaters (excreted during human therapy), as well as surface waters [3,4]. Conventional treatment methods (i.e. physical, chemical and biological) are inefficacious to remove this compound due to its chemical structure, additionally, CIP is unaffected under some conditions (T, pH) of biological treatments [5,6]. Thus, its presence is becoming a serious human risk in aquatic environments, since it is mainly associated with the proliferation of antibiotic resistant organisms [7], that can generate toxic effects to other organisms even at low concentrations [8]

Electrochemical oxidation technologies are efficient alternatives for CIP abatement [9,10], relying on the destruction of pollutants via strong oxidants (i.e. hydroxyl radicals, active chlorine, etc). The recent interest of active chlorine species (Cl_2-active, Cl_2/Cl^- E = 1.36 V vs SHE, $HClO/Cl^-$ E = 1.49 V vs SHE and ClO^-/Cl^- E = 0.89 V vs SHE) is connected to the presence of chloride ions in multiple effluents and wastewaters, whence it can be exploited as a natural reagent. The activity of Cl_2-active species occurs at less positive potentials compared to other oxidants, which makes it more selective for contaminants contained along with natural organic matter [11]. Additionally, the main functional groups of CIP (phenolic, tertiary aliphatic and aromatic amine moieties) are susceptible to undergo chlorine oxidation [12].

* Corresponding author. Tel.: +52 55 58044600x2686.
E-mail addresses: jorge_gva@hotmail.com, jgva@xanum.uam.mx (J. Vazquez-Arenas).
[1] CONACYT research fellow.

http://dx.doi.org/10.1016/j.electacta.2016.07.150
0013-4686/

Cl_2-active species are well-known to be efficiently generated via chloride oxidation on Dimensionally Stables Anodes (DSA). DSAs catalysts are comprised of an active noble metal oxide as catalyst (i.e. RuO_2) and a valve metal oxide as a stabilizer (i.e. TiO_2, SnO_2, Ta_2O_5). These anodes are distinguished by a high surface area, high catalytic activity, high stability to anodic corrosion, electrical resistance and low-energy consumption [13,14]. Concerning the synthesis of DSA anodes, the Pechini method remains as one of the preferred alternatives to fabricate them [15]. To some extent, this is largely due to its low cost, simplicity to coat non-uniform geometries of controlled thicknesses and low-temperature synthesis [16].

The electrochemical properties of DSAs based on RuO_2 can be synergistically modulated by controlling the composition of constituent oxides [17–19]. Wang et al. investigate the role played by the different Ru:Sn ratio in Ti/RuO_2-SnO_2 anodes, describing that the mixed oxide has a better electrochemical performance (Cl_2-evolution) than the sole RuO_2 in 0.5 M NaCl [20]. Da Faria et al. showed that a ternary DSA ($Ru_{0.3}$ $Ti_{0.7-x}Ce_xO_2$) was considerably more active for Cl_2 evolution than a binary electrode ($Ru_{0.3}$ $Ti_{0.7}$ O_2), as a result of active surface area [21]. The incorporation of ZrO_2 in a ternary oxide has been hardly studied in electro-catalysis [22–24]. This material presents a high corrosion resistance, excellent thermostability, and it can act as a "diluent" for RuO_2 improving the catalyst dispersion and number of active sites, in order to increase the electrochemical activity [25]. On the other hand, a small quantity of Sb_2O_5 is currently used as dopant to enhance conductivity and conformation within a ternary oxide [26,27].

Accordingly, ternary thin films of RuO_2, ZrO_2 and Sb_2O_5 are expected to be promising electrode materials for multiple electro-catalytic applications. To this concern, a stable Sb_2O_5 doped Ti/RuO_2-ZrO_2 catalyst (1:0.3:0.004 Ru: Zr: Sb) has been designed to degrade Indigo Carmine in a FM01-LC reactor and reactive black 5 at micro-electrolysis level [28,29]. Therefore, the aim of this work is to investigate the CIP degradation using Cl_2-active species electro-generated on a ternary Sb_2O_5-doped Ti/RuO_2-ZrO_2 (1:0.5:0.004 Ru: Zr: Sb molar ratio) anode. The role of ZrO_2 and Sb_2O_5 are evaluated upon the catalyst microstructure, and electro-catalysis performance in NaCl and Na_2SO_4 solutions. The byproducts resulting from the antibiotic degradation are identified by High Performance Liquid Chromatography (HPLC) and High Performance Liquid Chromatography- Mass Spectrometry (HPLC-MS). Quantum chemistry calculations are also conducted to identify the susceptible regions of Cl_2-active attacks within the CIP structure, and its feasible degradation pathways.

2. Materials and methods

2.1. Preparation of electrodes

A ternary Sb_2O_5-doped Ti/RuO_2-ZrO_2 (Ti/SbRuZr) anode was prepared using the Pechini method according to Palma-Goyes et al. [28]. Analytic grade reagents of $RuCl_3$, $ZrO(NO_3)_2{\cdot}2H_2O$ and $SbCl_3$ from Sigma-Aldrich were utilized as metallic precursors in a polymeric mixture prepared with a nominal molar ratio of 1:0.5:0.0004 (Ru:Zr:Sb), with 2.4 M citric acid as chelating agent, and 18 M ethyleneglycol as reaction solvent. Note that this ratio was found to generate the ternary catalyst with the highest capacity to electro-generate active chlorine species [30]. The polymeric mixture was kept stirred for 30 minutes at 80 °C and subsequently deposited on Ti plates (2 × 2 cm), which were previously treated in oxalic acid (Merck) at 75 °C for 30 min. These plates were dried at 180 °C and calcined at 550 °C for 1 h in a furnace. Both temperatures were selected from thermogravimetric analysis (TGA) and differential thermal analysis (DTA) data of the raw polymeric mixture (supplementary data 1). The coating procedure was repeated eight times to thicken the coating.

2.2. Microstructural characterization

Surface morphology and chemical composition of Ti/SbRuZr anode were determined by Field Emission Scanning Electron Microscopy-Energy Dispersive X-ray Spectroscopy (FESEM-EDS) with a SM-7600F microscope using an accelerating voltage of 10.0 kV. X-ray diffraction (XRD) data were collected with a PANalytical Empyrian diffractometer in a Bragg-Brentano (θ-2θ) configuration operated with a Cu Kα*1*/α*2* radiation (λ = 1.5418 Å) at 45 kV and 40 mA from 25 to 60° (2θ) using a PIXcel 3D detector. The crystalline phases were identified using the JCPDS-ICDD cards. The full width at half maximum (FWHM) value for average crystallite size calculation using the Scherrer equation was obtained from a profile refinement using the FULLPROF program.

2.3. Electrochemical behavior

Electrochemical studies were performed in a cylindrical three-electrode cell with a capacity of 130 mL. Ti/SbRuZr was used as working electrode, while a pure graphite rod (0.5 mm diameter × 16 mm length, Alfa AESAR, 99.999%) and Ag/AgCl (0.197 V vs SHE) were used as counter and reference electrode, respectively. Ti/RuO_2 was also studied as a working electrode for comparison purposes. The aqueous solutions subjected to electrolysis contained 0.151 mM (50 mg L^{-1}) ciprofloxacin (65% Laproff) and 0.05 M NaCl (Merck) as supporting electrolyte at pH 5. The cell was operated at room temperature by applying a constant current density of 17 mA cm^{-2}. These experiments were conducted with vigorously stirring to enhance mass transport toward the electrodes. Samples collected from electrolysis were quenched using 0.1 M Sodium metabisulfite ($Na_2S_2O_5$) before analytical testing.

Cyclic Voltammetry (CV) and Electrochemical Impedance Spectroscopy (EIS) experiments were obtained using a potentiostat/galvanostat Autolab PGSTAT 302N. Linear sweep voltammetry was carried out at a scan rate of 20 mV s^{-1} in the range from −0.5 to 1.6 V vs Ag/AgCl. EIS spectra were obtained in solutions containing 1.0 M H_2SO_4 at potentials of 1.2, 1.3 and 1.4 V. A wave amplitude of 10 mV was used because it was small enough to allow linearization of the response to the input signal, but also high enough to yield a response that was detectable from the measurement noise. The frequency was varied from 1 MHz to 0.01 Hz at 10 points per decade. Two replicate EIS experiments were conducted at each potential to verify the reproducibility of the measurements. Estimation of the electrochemically active surface area (ECSA) was attempted for each catalyst using the parameters (Table 1) obtained from the fitting of experimental EIS spectra [31], and its specific capacitance (i.e. smooth planar surface in a determined electrolyte). However, this procedure did not succeed since most

Table 1
Parameters obtained by fitting experimental EIS spectra recorded at different potentials for the Ti/RuO_2 and Ti/SbRuZr electrodes in 1 M H_2SO_4.

Electrode	E/V vs Ag/AgCl	R_1 Ω cm^2	Q_1 F cm^{-2} $s^n \times 10^{-3}$	n
Ti/RuO_2				
	1.2	6600	2.8	0.96
	1.3	63	2.0	0.94
	1.4	7.2	2.8	0.90
Ti/SbRuZr				
	1.2	4200	1.6	0.89
	1.3	162	1.8	0.90
	1.4	36	1.2	0.88

likely complex interfacial processes occur along with double layer formation including the deposition of catalysts on large polycrystalline Ti plates compared to typical electrode sizes, and the mixture of co-deposited phases (e.g. RuO_2, ZrO_2, Sb_2O_5) with different capacitive and charge-transfer properties.

2.4. DSA performance

The CIP concentration and degradation byproducts were monitored using HPLC in a reversed phase, in an UHPLC Thermo Scientific DIONEX UltiMate 3000. Thermo Scientific Acclaim 120 (C18 5 μm, 4.6 × 100 mm) and 0.02 M formic acid (CH_2O_2) at pH 2.7 along with acetonitrile (85:15 v/v) was used as stationary and mobile phase, respectively. The system was operated isocratically at a flow rate of 1.0 mL min^{-1}. The sample was injected through a fixed sample loop having a volume of 20 μL. The diode array (DAD) detector was set at 277 nm. HPLC-MS analysis was carried out using an Agilent Chromatograph equipped with a UV-visible photodiode array 136 detector and atmospheric-pressure ionization (API) chamber working in positive mode using a reverse phase column Zorbax eclipse XDD-C18, 4.6 × 150 mm, 5 μ.

CIP mineralization was monitored using a Total Organic Carbon (TOC, mg $L^{-1}C$) analysis in a 5000A Shidmazu equipment, with a solution of potassium hydrogen phthalate as calibration. Acidification and stripping before analyses were performed to keep a CO_2 free-environment.

Evolution of Cl_2-active was determined iodometrically [32]. Aliquots taken from the reactor were added to a quartz cell containing potassium iodide (0.1 M) and ammonium heptamolybdate (0.01 M). The absorbance was recorded at 350 nm after 2 minutes of reaction. To avoid interferences, absorbance of CIP was also measured at 350 nm, under the same conditions, and the

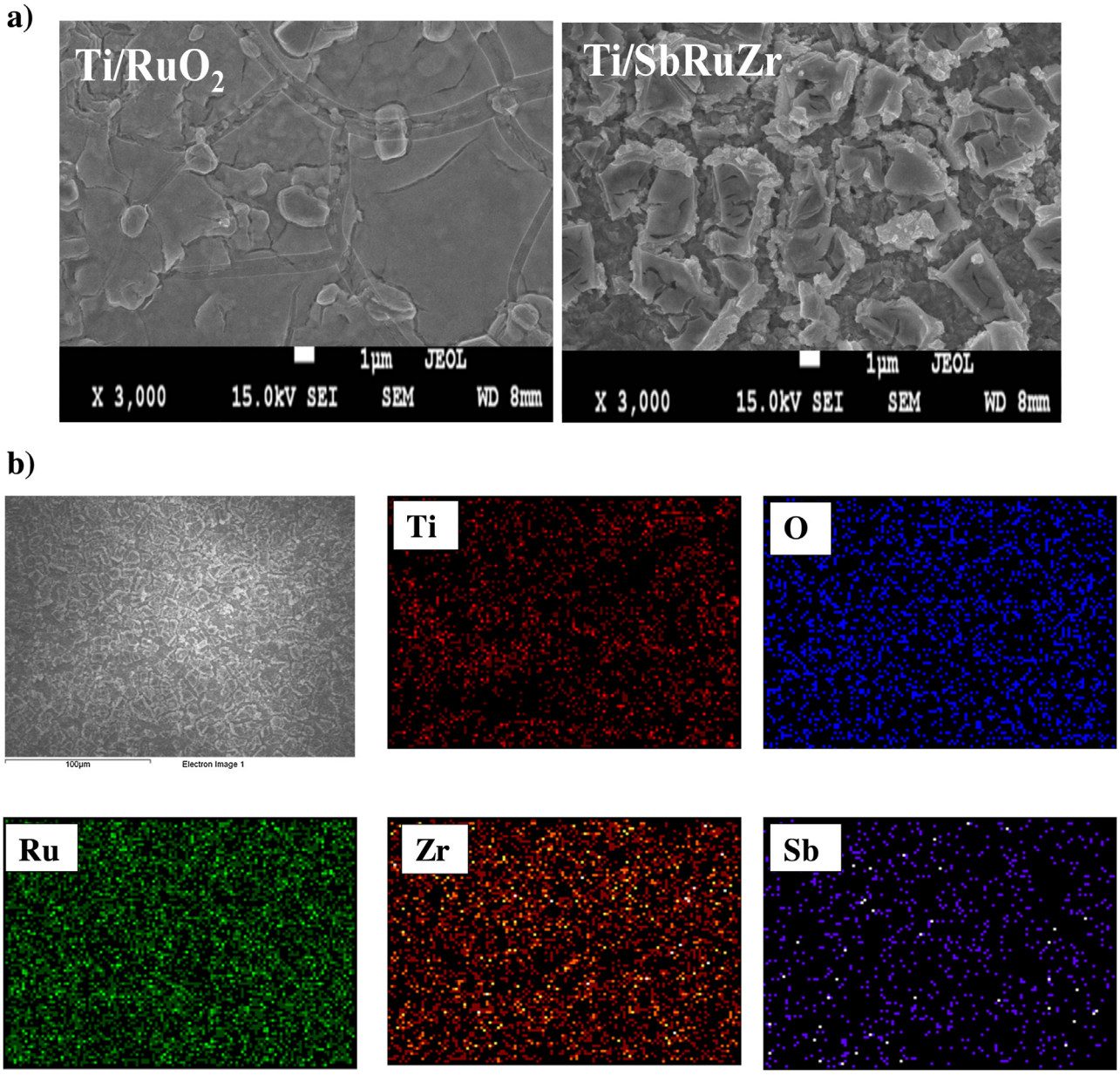

Fig. 1. a) SEM images of Ti/SbRuZr and Ti/RuO_2 electrodes, b) Mapping showing distribution of Ti, O, Ru, Zr and Sb elements on Ti/SbRuZr electrode.

obtained value was taken into account to the quantification of these Cl_2-active. The formation rate of Cl_2-active ($\mu M\ min^{-1}$) was determined by linearizing the graph of evolution of Cl_2-active (μM) vs electrolysis time (min). This rate is an indicative of the amount of oxidizing agent formed per unit of time on the anode surface. Unfortunately, the faradaic efficiency could not be determined for the formation of active chlorine via conventional rotating ring-disk electrode technique, since it concurrently occurs with OER.

The antibiotic activity (AA) was measured for the treated samples to evaluate whether or not CIP byproducts maintained biological activity. Thus, 30 μL of these samples were inoculated in agar plates with a 10^5 CFU mL^{-1} suspension of *Staphylococcus aureus* (ATCC 6538), as the probe microorganism. The plates were then incubated for 24 h at 37 °C. The inhibition halo, in mm, was measured and compared to the control assay made with pure solutions of antibiotic and microorganism [33].

2.5. Computational details

Theoretical calculations of topological and natural orbitals of CIP molecular structure and its main intermediates were computed to propose an electrochemical oxidation pathway for degradation. Density functional theory was initially employed to compute the optimized structures and frequency analyses using the B3LYP hybrid density functional [34]. All calculations were conducted using the 6-31+g(d) basis set, and the polarized continuum model (PCM) [35] using the dielectric constant for water, as implemented in Gaussian 09, Revision D.01. The regions or atoms of CIP molecule and its main degradation intermediates susceptible to undergo electrophilic attack were assigned by topological analysis using the Fukui function, which is represented as $f^-(r)$, and through the natural bond orbital analysis, which evaluate the total charge in the atoms.

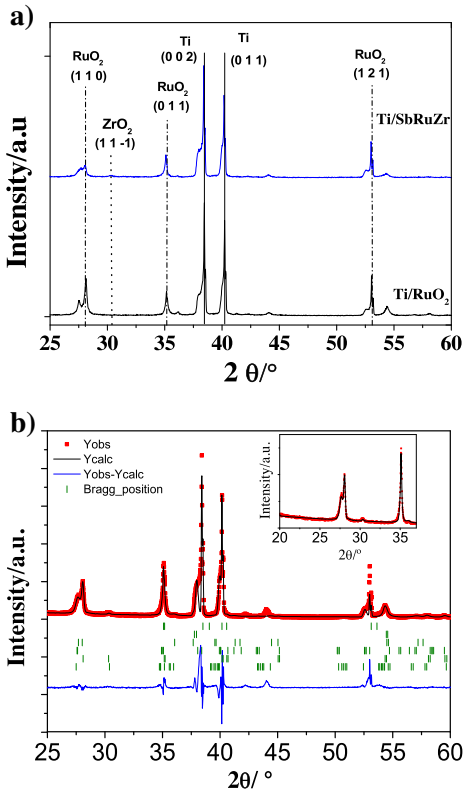

Fig. 2. a) XRD pattern of Ti/SbRuZr and Ti/RuO_2 electrodes. b) Profile refinement fit conducted for the Ti/SbRuZr electrode. Tick marks indicate positions related to Bragg reflections: first two upper marks are associated with Ti (*P6/mmm*), TiO_2 (*P4/mmm*), RuO_2 (*P4₂/mmm*) and ZrO_2 (*P2/m*) structures. Bottom lines correspond to the differences found between experimental and calculated patterns. The inset shows a Bragg angle region from 20 to 35°.

3. Results and discussion

3.1. Microstructural characterization

Fig. 1a shows SEM micrographs of the synthesized Ti/SbRuZr and Ti/RuO_2 electrodes. As observed, Ti/RuO_2 exhibits a compact coating conformed of small agglomerated particles with an island-type shape and cracks distributed along the electrode surface. These characteristics have been observed for similar oxide systems obtained by thermal decomposition methods [36]. The electrode morphology becomes heterogeneous when ZrO_2 and Sb_2O_5 are added to the RuO_2 coating (Ti/SbRuZr), although the primary particle distribution is preserved. EDS analyses of the ternary oxide were carried out in a $100 \times 100\ \mu m$ area, and these results confirmed the presence of Ru, Zr and Sb elements (17, 10 and 1 at. %,

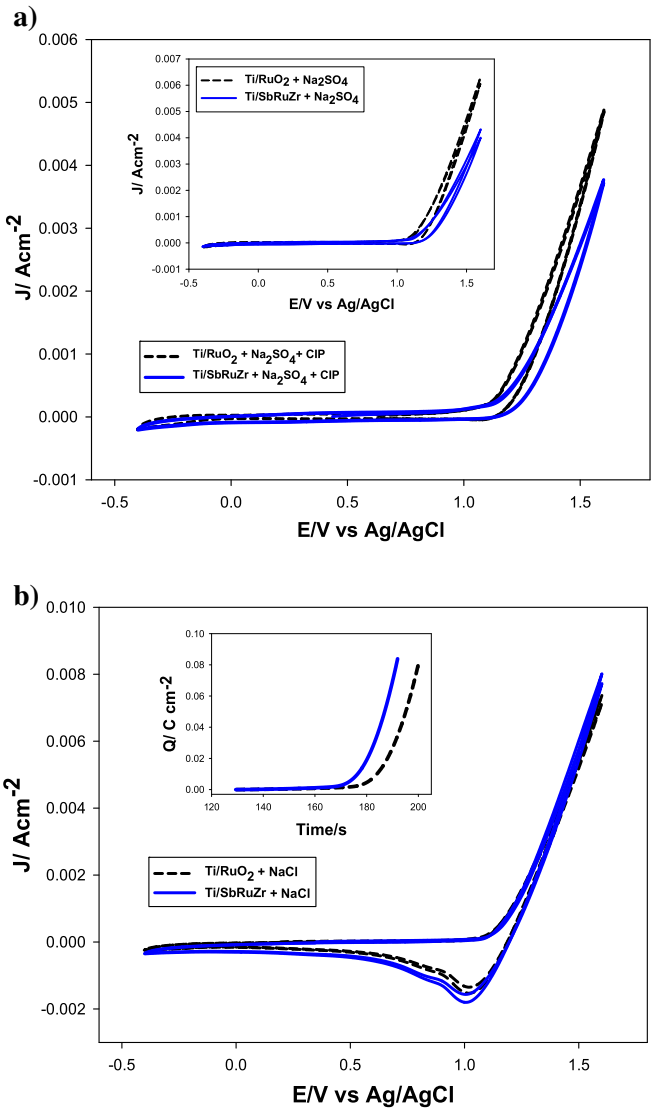

Fig. 3. Cyclic voltammetry conducted on Ti/SbRuZr and Ti/RuO_2 anodes in different supporting electrolytes: a) 0.05 M Na_2SO_4 with and without CIP (inset), b) 0.05 M NaCl. Inset of 3b: charge associated with the oxidation process as a function of time in NaCl. Scan rate: 20 mVs^{-1}, pH 5.

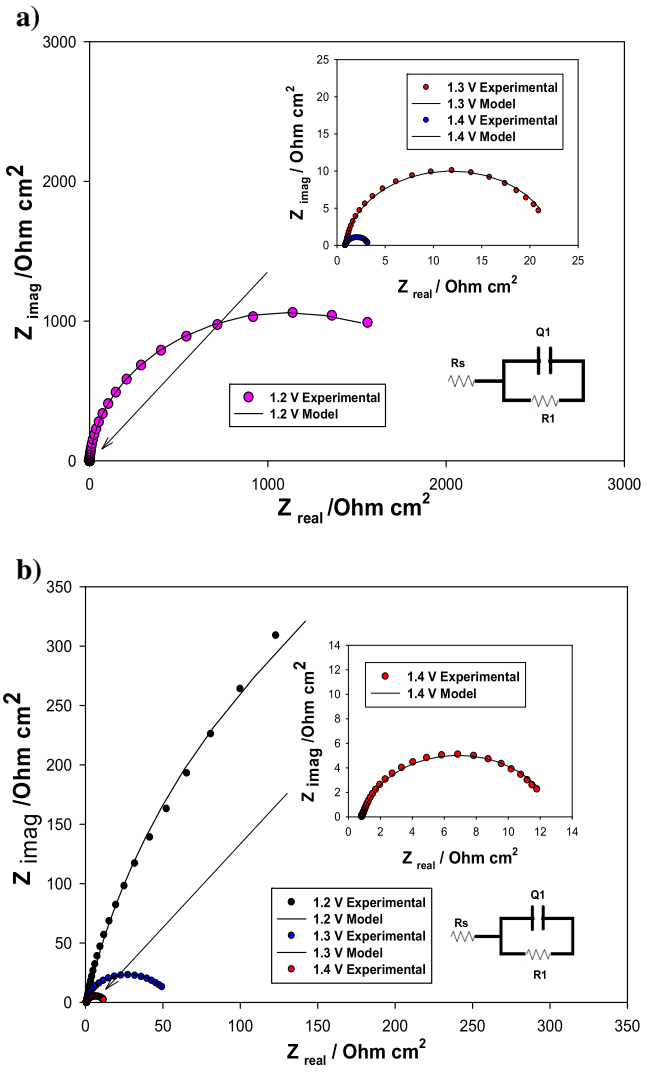

Fig. 4. Nyquist plots obtained for a) Ti/RuO_2 and b) Ti/SbRuZr anodes measured at 1.2, 1.3 and 1.4 V during the occurrence of OER in 1 M H_2SO_4. Inset: zoom of 1.3 and 1.4 V spectra. Solid curves are the fits of experimental data using the equivalent electric circuit displayed in the figure.

respectively). Likewise, Fig. 1b shows the mapping distribution of the elements onto the electrode surface, evidencing a high dispersion of each of them along the coating.

Fig. 2a shows XRD patterns of Ti/SbRuZr and Ti/RuO_2 anodes. The analysis conducted to identify the crystalline phases (supplementary data 2) revealed the presence of RuO_2 (05-1159) and ZrO_2 (01-5983). Sb_2O_5 phase was not detected due to the lowest molar content used to fabricate the electrode. These metallic oxides grew up on a layer of TiO_2 rutile (00-9161), previously formed on Ti substrate (04-3416). Note that predominant peaks are characteristic of tetragonal crystalline structure ($P4_2/mmm$): 2θ = 28, 35 and 54 attributed to (1 1 0), (0 1 1) and (1 2 1) reflection planes, respectively. The above observation suggests that TiO_2 layer could orient the RuO_2 growth, mainly favored for their similar lattice parameters. On the other hand, the peaks associated to ZrO_2 ($P2/m$): 2θ = 27 and 31 attributed to (1 1 -1) and (1 1 1) reflection planes indicated a co-deposit of RuO_2 and ZrO_2 oxides into the coating, and thereby a solid solution is excluded. Fig. 2b shows the profile refinement fit conducted for Ti/SbRuZr to obtain a more accurate description of its microstructure. The average crystallite size for both electrodes (Ti/SbRuZr and Ti/RuO_2) was calculated through Scherrer equation (Eq. (1)):

$$\tau = \frac{0.9\lambda}{\beta cos\theta} \quad (1)$$

where τ is the mean grain size, λ is the X-ray wavelength, β is the full-width at half maximum (FWHM) and θ is the Bragg angle. The FWHM was determined via Caglioti function using the U,V,W peak shape functions obtained from the refinement previous instrumental correction with a LaB_6 NIST standard. The inset of Fig. 2b shows the selected (110) plane for FWHM calculation of the tetragonal-type RuO_2 structure. Results obtained from Scherrer equation show that average crystallite size of the ternary oxide decreases drastically when ZrO_2 is present (109 and 61.2 nm for Ti/RuO_2 and Ti/SbRuZr, respectively). A decrease of the crystallite size could modify the surface area of the coating, which on its turn seems to affect the catalytic activity of the synthesized materials.

3.2. Electrochemical behavior

One of the main electrochemical properties desired in DSAs is closely related to their degradation capacities towards organic compounds. In this direction, the degradation mechanism on DSAs may proceed directly on their surfaces, or indirectly through the electro-generation of an oxidizing agent on the anode [37]. Thus, electrochemical characterizations of Ti/SbRuZr and Ti/RuO_2 were carried out in solutions containing 0.05 M NaCl and 0.05 M Na_2SO_4. Note that two different electrolytes (with and without chloride ions) were used to assess the occurrence of oxygen evolution reaction (OER) in Na_2SO_4, and its competence against active chlorine formation (NaCl). Fig. 3 shows cyclic voltammograms obtained for Ti/SbRuZr and Ti/RuO_2 in the absence (inset) and presence of 0.15 mM CIP (main plot) in Na_2SO_4. As observed in Fig. 3a, the predominant process in the absence of CIP is OER for both electrodes (Eqs. (2)–(4)) [38]:

$$MO_x - H_2O_{ads} \rightarrow MO_x(e^-) - OH^{\circ}_{ads} + H^+ \quad (2)$$

$$MO_x - OH^{\circ}_{ads} \rightarrow MO_{x+1} + H^+ + e^- \quad (3)$$

$$MO_{x+1} \rightarrow MO_x + \frac{1}{2}O_2 \quad (4)$$

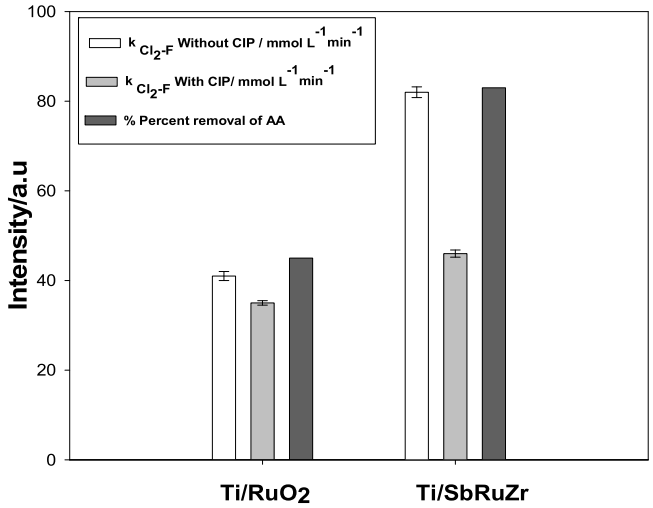

Fig. 5. Removal of antibiotic activity of CIP, and active chlorine evolution during the electrochemical treatment. k_{Cl2-F} is the formation rate of active chlorine species.

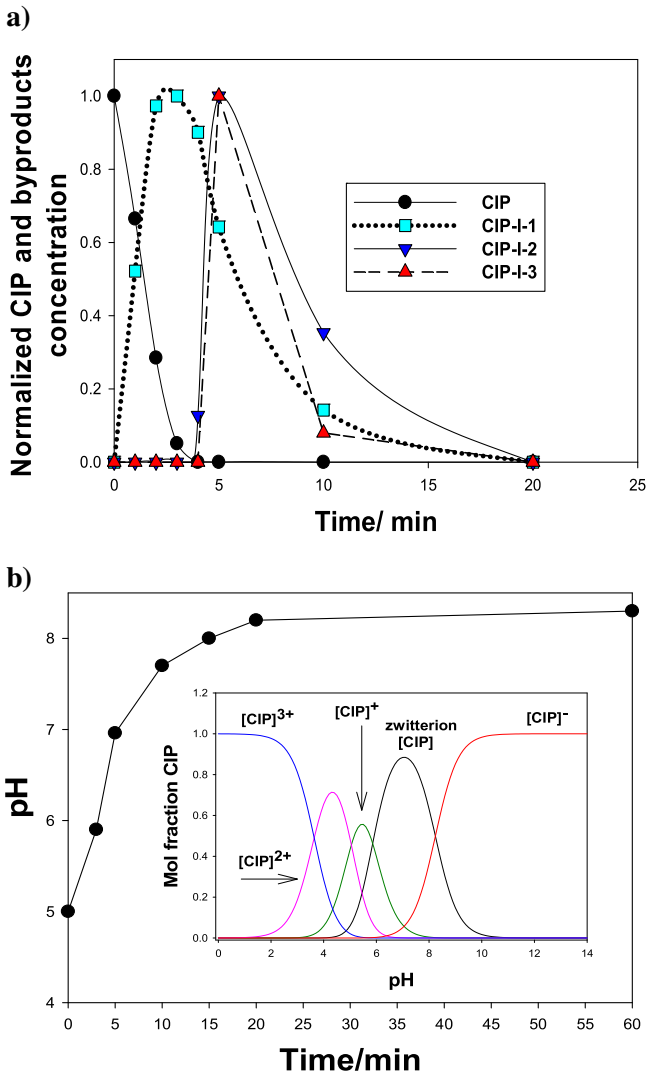

Fig. 6. a) Byproduct (CIP-I-1, CIP-I 2 and CIP-I-3) concentrations as a function of time during electrochemical treatment for CIP. b) pH evolution during electrochemical treatment. Inset of 6b: thermodynamic diagram (Fraction of CIP vs pH) displaying the predominant and coexisting species of CIP as a function of pH.

$$MO_{x+1} + R \rightarrow MO_x + RO \quad (5)$$

where MO_x represents the anode materials: Ti/RuO_2 or ternary oxides, MO_{x+1} the oxidized material due to electrolysis, while R and RO represent organic and oxidized organic compounds, respectively. A similar behavior was obtained for both electrodes when CIP was present in the solution, indicating that a direct oxidation (Eq. (5)) did not occur during the electrochemical treatment. In addition, the current density for Ti/RuO_2 is higher than for Ti/SbRuZr at the same potential value, providing strong evidence to consider that Ti/RuO_2 is a better catalyst to perform the OER. The same behavior is described in the absence of CIP (inset of Fig. 3a).

On the other hand, a cathodic wave around 1.0 V is recorded for Ti/RuO_2 and Ti/SbRuZr electrodes when NaCl was used as electrolyte in the absence of CIP (Fig. 3b). This process is attributed to active chlorine reversible processes (e.g. Cl_2/Cl^- couple), stemmed from the previous chlorine formation during anodic scan according to Eqs. (6)–(7) (standard potential of 1.17 V) [39]:

$$MO_x - OH^{\circ}_{ads} + Cl^- \rightarrow MO_x(HClO) + e^- \quad (6)$$

$$MO_x(HClO) + Cl^- \rightarrow MO_x + \frac{1}{2}Cl_{2(g)} + OH^- \quad (7)$$

Therefore, the formation of Cl_2-active species along with a possible sluggish water oxidation could be used to degrade CIP in solution, as verified in the difference of overpotentials and current densities obtained from OER processes occurring in Fig. 3a and b. Moreover, chlorine reacts with water to get hypochlorous acid and hypochlorite ions depending on pH according to Eqs. (8) and (9) [40]:

$$Cl_2 + H_2O \rightarrow HClO + Cl^- + H^+ \quad (8)$$

$$HClO \rightarrow ClO^- + H^+ \quad pK_a = 7.5 \quad (9)$$

Voltammetry studies of DSAs containing SnO_2 instead ZrO_2 (Ti/RuO_2-Sb_2O_5-SnO_2) in NaCl and Na_2SO_4 electrolytes have shown that chlorine evolution occurs more facile than oxygen evolution [41], and this reaction could initiate at lower overpotentials depending on Cl^- concentration. Under this premise, a comparison of the charge (Q, i.e. number of moles electrolyzed) associated with the oxidation processes was determined for both electrodes in 0.05 M NaCl (inset of Fig. 3b). As observed in the inset of Fig. 3b, the onset of Q increase occurs at lower overpotentials for Ti/SbRuZr than Ti/RuO_2, confirming that the reaction rate to form Cl_2-active is higher for the ternary oxide. As discussed above, water oxidation occurs more feasibly on Ti/RuO_2, but the opposite happens to form Cl_2-active on this surface. Presumably, the opposite behavior arises on Ti/SbRuZr electrode, but requires further validation. Accordingly, these results could indicate that the key role of an efficient catalyst to form Cl_2-active is its capacity to increase the onset overpotential for water oxidation. This finding requires further confirmation with a more sensitive technique to determine charge transfer reactions.

EIS studies were carried to get information of the charge transfer resistance for the OER occurring on Ti/SbRuZr and Ti/RuO_2 electrodes. In recent years, this technique has been utilized to measure faradaic and non-faradaic phenomena and it is able to deconvolute processes occurring at similar rates. EIS has been commonly used to analyze the structural and electronic properties of anode materials, although its use in electrocatalysis has been mainly focused on evaluating the resistance of electrochemical reactions (i.e. charge transfer) employing equivalent circuits, which is a tractable way to assess EIS diagrams. Therefore, EIS measurements were carried out to study water oxidation in electrolytes containing 1.0 M H_2SO_4, in order to test the hypothesis that this reaction occurs more facile on Ti/RuO_2. This reaction has been preferred over chlorine evolution since it takes place solely from other faradaic contributions. Fig. 4 shows Nyquist spectra obtained on a) Ti/RuO_2 and b) Ti/SbRuZr electrodes under potentiostatic mode at 1.2, 1.3 and 1.4 V. These potential values were selected to ensure the occurrence of water oxidation (refer to Fig. 3a). As observed in Fig. 4, the components of impedance become lower as the potential is made more positive, suggesting that the activation barriers of OER are more easily overcome by the application of a higher energy. When this process is completely noticeable, the resistive contributions (Z real) are higher than the capacitive ones (Z imaginary) indicating that the rate-controlling step could be associated with the charge transfer resistance of water oxidation. A similar behavior has been described in the literature, where the arc located at high frequencies corresponds to an electron-transfer limited process [42]. A comparison of the components of impedance for both substrates reveals that lower values are obtained on the Ti/RuO_2 electrode, whereby water

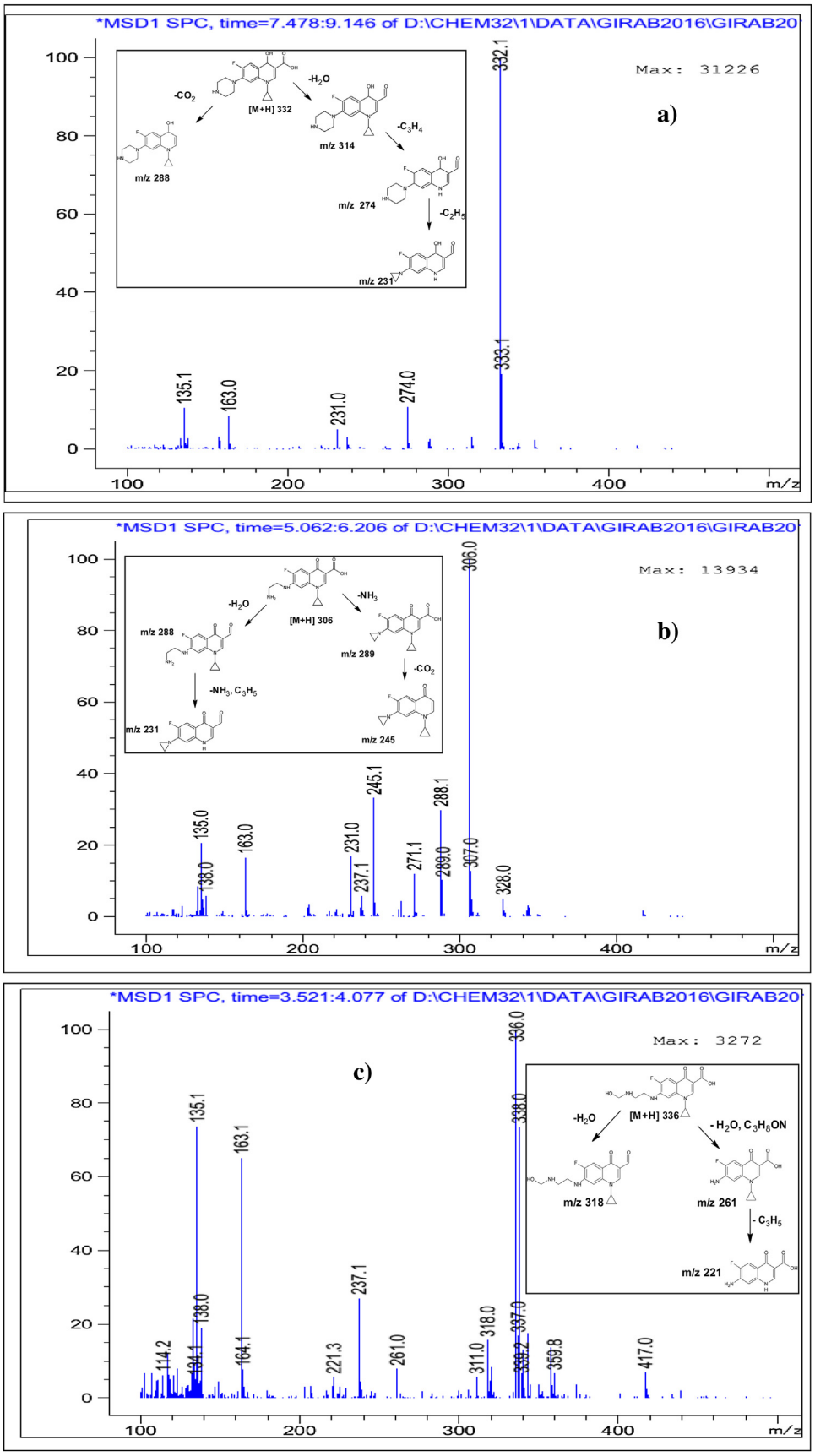

Fig. 7. MS-ESI+ spectra for CIP and main byproducts generated from the electrochemical treatment in chloride media.

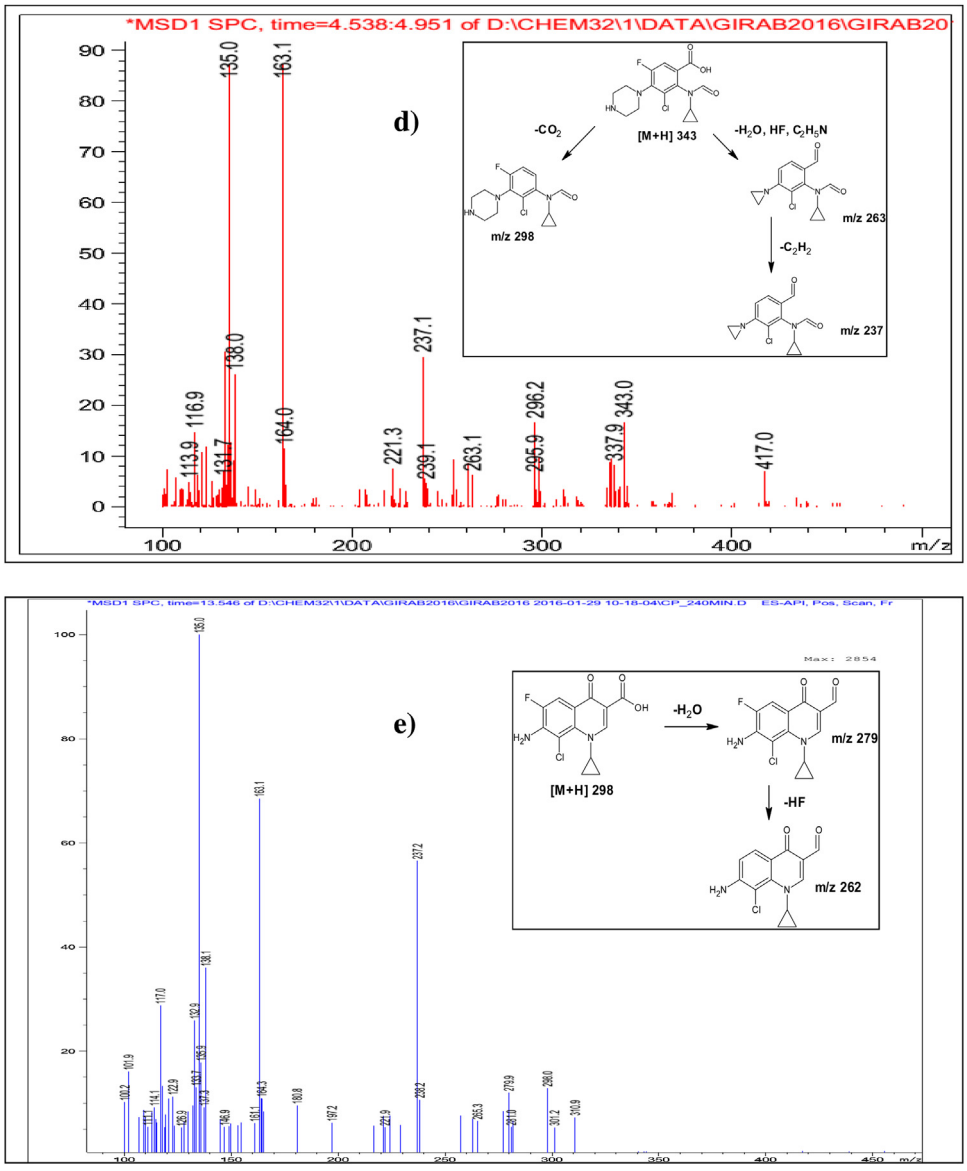

Fig. 7. (Continued)

oxidation could be more catalytic on this substrate compared to Ti/SbRuZr electrode. Table 1 shows the parameters obtained from the fitting of the equivalent circuit to the experimental spectra for the catalysts. A simple array $R_s(R_1Q_1)$ was used as equivalent circuit for these purposes, where R_s and R_1 are the electrolyte resistance and the charge transfer resistance of water oxidation, respectively; and Q_1 is a constant phase element connected to an heterogeneous double-layer capacitance of the anode/electrolyte interface. As observed in Table 1, the Q_1 values are not significantly modified between both electrodes, but the charge transfer resistance (R_1) obtained for Ti/RuO_2 is one order of magnitude lower compared to the Ti/SbRuZr anode. This result confirms that the occurrence of water oxidation is more catalyzed on Ti/RuO_2 than on the ternary material, as evaluated in the voltammetry analysis (Fig. 3). It is worthwhile mentioning that although the roughness of materials influences the impedance values, RuO_2 substrate is considerably smoother (refer to Fig. 1a) whence its impedance components are expected to be lower (i.e. lower real area) compared to Ti/SbRuZr catalytic. Thus, the same catalytic trend above described would be observed.

3.3. Degradation of ciprofloxacin in aqueous media

3.3.1. Monitoring of antibiotic activity

The capacity of Ti/SbRuZr for CIP degradation was compared to Ti/RuO_2 by monitoring its antibiotic activity. Degradation tests were carried out in solutions containing 0.15 mM CIP and 0.05 M NaCl for 20 min of electrochemical treatment, applying a current density of 17 mA cm^{-2} under constant stirring. Fig. 5 shows the results obtained for the removal of AA using Ti/SbRuZr and Ti/RuO_2 anodes, and the formation rate of Cl_2-active in absence and presence of CIP for both of them. As observed, the Ti/SbRuZr electrode removed up to 83% of AA after 30 min (0.19 AhL^{-1}), while only 45% was eliminated on Ti/RuO_2. In addition, the formation rate of Cl_2-active in absence of CIP was greater for Ti/SbRuZr electrode (81.0 ± 1.2 μM min^{-1}) than for Ti/RuO_2 (41 ± 1.0 μM min^{-1}), while

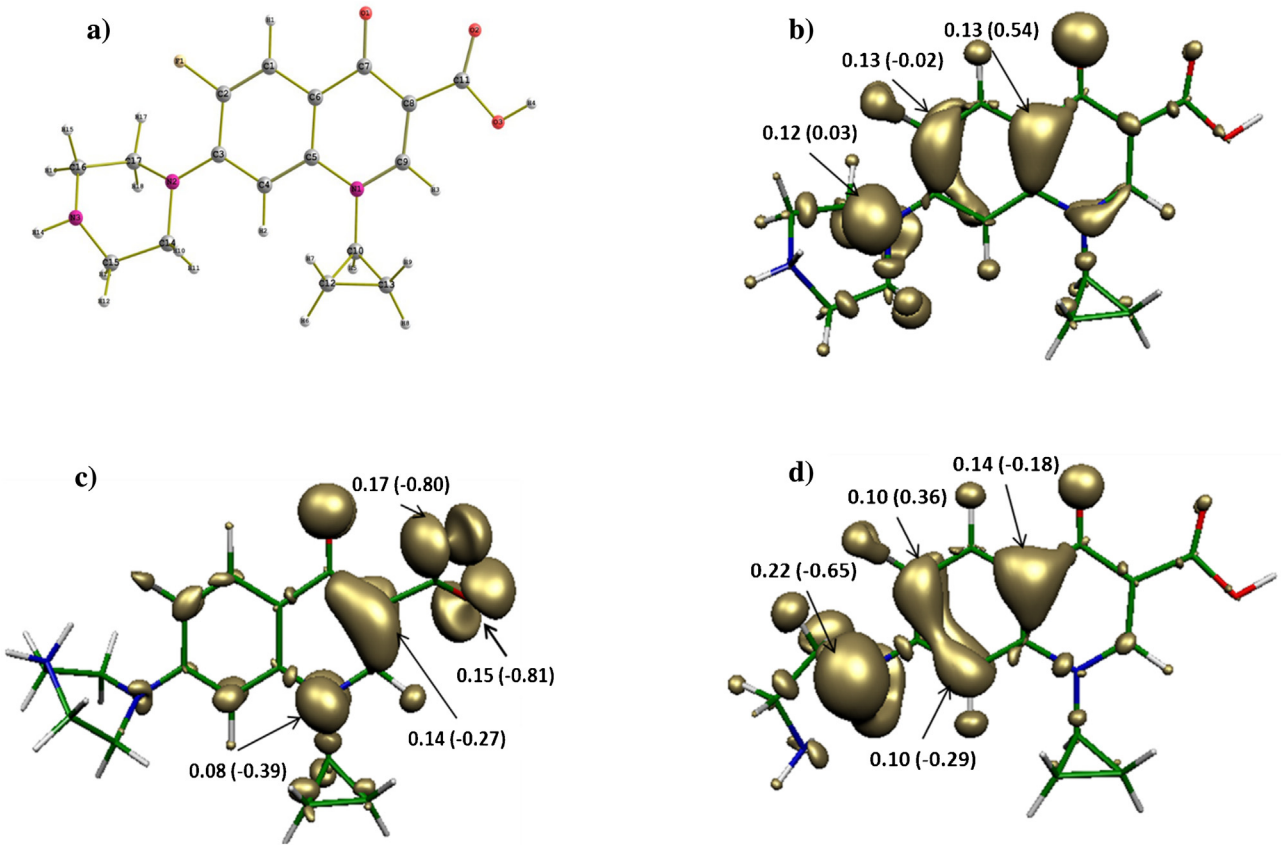

Fig. 8. Surface plots displaying condensed nucleophilic Fukui functions computed for the fundamental states (B3LYP/6-31+g(d)) of CIP, and its main degradation byproducts. The natural charge values calculated from the natural bond orbital analysis are presented in brackets: a) CIP, b) $[CIP]^+$, c) Zwitterion CIP, d) CIP-I-1.

this value becomes lower for both catalysts in the CIP presence: Ti/SbRuZr ($46\pm$ 0.80 μM min^{-1}) and for Ti/RuO_2 (35 ± 0.25 μM min^{-1}). These results suggest that the main degradation pathway for CIP and its associated removal of AA in both electrodes involves the action of Cl_2-active. A complete removal of AA was obtained for Ti/SbRuZr electrode after 60 minutes, which can be mainly attributed to modifications of the quinolone moiety or peripheral moieties (piperazine ring, cyclopropyl, carboxyl group and fluorine) that play important roles in antibiotic activity.

3.3.2. Degradation pathway of CIP electro-oxidation

HPLC-MS and HPLC-DAD analyses were conducted to monitor CIP degradation and its main intermediates resulting from the electrochemical treatment in chloride media, and their correlation with the removal of AA. The mechanism of CIP degradation was only evaluated on Ti/SbRuZr since the degradation pathway is the same for both electrodes (indirect by Cl_2-active), and only kinetic rates differ each other. Fig. 6 shows the course of CIP degradation, evidencing that its concentration exponentially decreases in five minutes, following a first-order kinetics, and the quick formation of intermediates that were generated during treatment (inset of Fig. 6a). The chromatograms obtained at different times of CIP degradation are shown in supplementary data 3. Although these intermediates are continuously accumulated, likewise, they are gradually destroyed to form other compounds, but they do not have any antibiotic activity as discussed in section 3.3. UV–vis spectra for CIP and some of its main intermediates are described in supplementary data 4. For CIP, distinctive UV absorption bands are located at 280 (λ_{max}, Peak I, $\pi - \pi^*$) and 330 nm (weak Peak II, n $-\pi^*$), where $\pi-\pi^*$ electron transitions (K-band) are mainly due to the aromatic ring absorption, while $n-\pi^*$ electron transitions (R-band) are caused by equilibrium of quinolones forming an intermolecular hydrogen bond with water solvent (hydrogen bond of the 4-keto and the 3-carboxylic acid group) [43], respectively. During the course of degradation, absorption bands associated to CIP disappeared and new profiles in the UV spectrum were obtained. This behavior suggests that the ring double conjugation in the quinolone moiety or peripheral moieties were degraded during the treatment, and it evidences susceptible sites within the CIP molecule for the attack of Cl_2-active species (Fig. 6a). Fig. 7 summarizes the mass spectrum (HPLC-MS) of CIP and the main intermediates CIP-I-1 (7-((2-aminoethyl)amino)-1-cyclopropyl-6-fluoro-4-oxo-1,4-dihydroquinoline-3-carboxylicacid, $C_{12}H_{12}FN_3O_3$, m/z 306), CIP-I-2 (1 cyclopropyl-6-fluor-7-((2-(hydroxymethyl)-amino)-ethyl)-amino)–4–oxo-1,4-dihydroquinoline-3-carboxil acid, $C_{16}H_{18}FN_3O_4$, m/z 336), CIP-I-3 (3-chloro-2-(cyclopropyl(formyl)amino)-5-fluoro-4-(piperazin-1-yl) benzoic acid, $C_{10}H_6ClFN_2O_3$, m/z 343) and CIP-I-4 (7-amino-8-chloro-1-cyclopropyl-6-fluoro-4-oxo-1,4 dihydroquinoline-3-carboxil acid, $C_{10}H_6ClFN_2O_3$, m/z 298). The molecular ion fragmentations and chemical structures for each compound were also included.

On the other hand, CIP molecule could present different ionic forms depending on the pH of the solution, as a result of its four pKa values (supplementary data 5) [44]. However, only two ionic forms were considered since the initial pH at 5.1 increased drastically in the first ten minutes of treatment (Fig. 6b). Under these conditions, the protonated (CIP^+) and zwitterion forms of CIP predominate in the electrolyte as observed in the inset of Fig. 6b. To

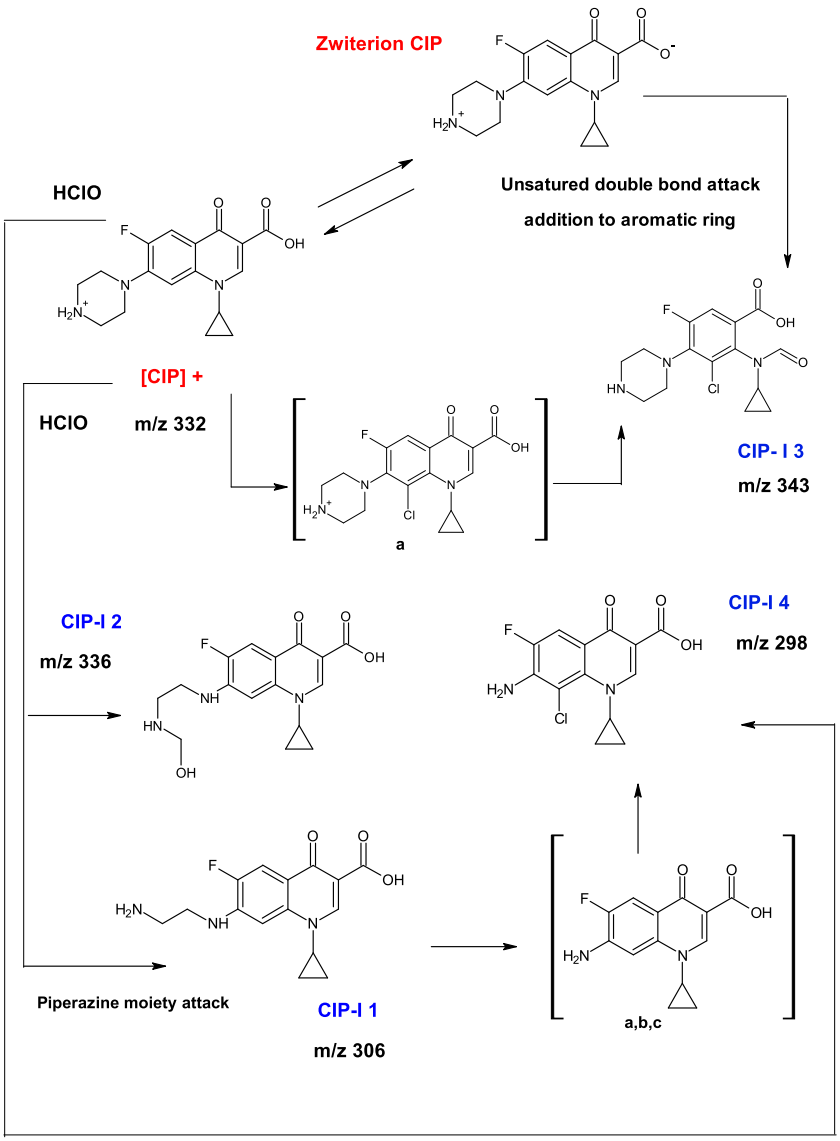

Scheme 1. Degradation pathway proposed for CIP throughout Cl_2-active species electro-generated on Ti/SbRuZr anode. a: Obtained by HPLC-MS in agreement with data reported by Dodd et al. [46]. b: Obtained by HPLC-Ms in agreement with data reported by Antonin et al. [49]. c: Obtained by HPLC-MS in agreement with data reported by An et al. [45].

this concern, these species were considered in a quantum chemical analysis which was performed to infer the position of electrophilic attacks, and elucidate possible stages of the degradation mechanism. This theoretical evaluation was focused on the electrophilic attack and unsaturated sites, since HClO $\left(Cl^{\delta+} + OH^{\delta-}\right)$ reactivity is regularly constrained to this type of sites. In addition, the analysis was also focused on the site with lowest steric impediment. Fig. 8 shows the values of Fukui functions and natural bond orbital (NBO) analyses for each region of protonated (Fig. 8b) and zwitterion (Fig. 8c) CIP as initial molecules, which are expected to be the most probable intermediates generated from the electrophilic attack of CIP. Note that lobes in this plot with a larger volume are more susceptible to undergo an electrophilic attack and the value in brackets is the charge of the atoms. Since these analyses suggest different sites depending on CIP forms, they were confronted against experimental HPLC-MS results for a more convincing evaluation of the reactive sites.

As discussed in Fig. 6b, CIP^+ and zwitterion species are the predominant ionic forms. For protonated CIP^+, theoretical studies revealed that the site located in the N2 atom within the piperazine group (Fig. 8b) is the most likely region to suffer a HClO attack via an initial Cl^+ transfer to the N2 atom, to yield a chloronium ion followed by addition of OH ion, leading to the rupture of the N2-C14 bond, and subsequently loss of C_2H_4, HCl and water to form CIP-I-1 (Scheme 1). This intermediate was generated during the first two minutes of treatment, has been also reported for other degradation processes. For instance, CIP-I-1 was found by An et al. during the CIP degradation conducted with several free radicals: OH, N_3 and SO_4^-; and Dodd et al. during water chlorination processes of fluroquinolones [43,44]. On the other hand, the attack of N2 atom of the piperazine moiety formed the intermediate CIP-I-2 ($C_{16}H_{18}FN_3O_4$, m/z 336) at longer exposures in accordance with the experimental HPLC-MS. This intermediate was found by Xiao et al. in the CIP degradation via Fenton process [47]. For the zwitterion CIP species, the deprotonated COO^- group favors the attack in the atom C8 of the quinolone moiety corresponding to unsaturated double bond C8-C9 (Fig. 8c). This behavior was found by H. Ou et al. during CIP degradation using UV and UV/H_2O_2 via multiple-wavelength ultraviolet [48]. A consecutive oxidation of

unsaturated double bond on quinolone moiety by cleavage of double bond C8-C9 leads to intermediate CIP-I-3 ($C_{10}H_6ClFN_2O_3$, m/z 343), which subsequently endured a chlorine electrophilic addition into aromatic ring. Intermediate CIP-I-4 ($C_{10}H_6ClFN_2O_3$, m/z 298) appeared after 120 min as a consequence of the successive degradation of intermediate CIP-I-1 on N2 according to Fukui analysis. This intermediate was also found by An et al., Dodd et al. and Yahya et al. [47,43,44]. After four hours of electrochemical treatment, only 40% of total organic carbon was removed (not shown). The accumulation of intermediates associated with this process indicates that despite of an incomplete degradation of quinolone moiety obtained during the treatment, the electro-conversion to aliphatic or aromatic compounds was achieved. Thus, the removal of AA is mainly attributed to the breaking and modification of CIP functional moieties.

4. Conclusions

A Ti/SbRuZr electrode prepared by Pechini method was microstructurally and electrochemically characterized to evaluate its performance towards ciprofloxacin degradation. SEM images and a profile refinement from XRD data demonstrated that Ti/SbRuZr consisted of dispersed phases formed by RuO_2 rutile (*P4/mmm*) and ZrO_2 monoclinic (*P2/m*). The presence of ZrO_2 decreased by twice the average crystalline size compared to Ti/RuO_2, which could improve the active area of the anode. CV (with and without CIP) and EIS studies revealed that Ti/SbRuZr surface acted as a catalyst to generate active chlorine species, leading to the removal of antibiotic activity without a complete CIP mineralization. Additionally, Ti/SbRuZr yielded a higher Cl_2-active concentration compared to Ti/RuO_2 due to its higher charge transfer resistance for oxygen evolution reaction. Quantum chemical calculations using DFT were combined with HPLC-MS results to propose a reaction pathway for CIP degradation, and to identify the active sites of CIP undergoing an attack of Cl_2-active species. Different degradation pathways were determined for the protonated and zwitterion (i.e. predominant initial molecules) ionic forms of CIP. Four intermediates were elucidated during CIP abatement, and this transformation involved the oxidation of unsaturated double bond on quinolone moiety (intermediate CIP-I-3), or rupture of piperazine moiety (intermediate CIP-I-1 and CIP-I-2) as a consecutive oxidation pathway. Valuable 40% of CIP mineralization was achieved to position the electrochemical oxidation as a promissory technology for improving the removal of quinolone compounds throughout Cl_2-active species.

Acknowledgments

Financial support is greatly appreciated from COLCIENCIAS (projects No. 111565843400 and 111565842980), convocatoria 658, 2014; SECITI-CDMX-MEXICO (Grant No. 2016-272), and Universidad de Antioquia (Sostenibilidad Program 2014-2015, Colombia). R. Palma-Goyes would like to thank COLCIENCIAS, Convocatoria No. 567-2012 for the financial support to pursue his Ph.D. J. Vazquez-Arenas also acknowledges the Cátedras-CONACYT (Mexico) program via project No. 1456, and Grant No. 2014-237343.

Appendix A. Supplementary data

Supplementary data associated with this article can be found, in the online version, at http://dx.doi.org/10.1016/j.electacta.2016.07.150.

References

[1] D. Fatta-Kassinos, S. Meric, A. Nikolaou, Pharmaceutical residues in environmental waters and wastewater: current state of knowledge and future research, Anal. Bioanal. Chem 399 (2011) 251–275.
[2] X. Van Doorslaer, J. Dewulf, H. Van Langenhove, K. Demeestere, Fluoroquinolone antibiotics: an emerging class of environmental micropollutants, Sci. Total Environ. 500–501 (2014) 250–269.
[3] S. Harris, C. Morris, D. Morris, M. Cormican, E. Cummins, The effect of hospital effluent on antimicrobial resistant E. coli within a municipal wastewater system, Environ. Sci. Process. Impacts 15 (2013) 617.
[4] T.G. Vasconcelos, K. Kümmerer, D.M. Henriques, A.F. Martins, Ciprofloxacin in hospital effluent: Degradation by ozone and photoprocesses, J. Hazard. Mater. 169 (2009) 1154–1158.
[5] N.M. Vieno, H. Härkki, T. Tuhkanen, L. Kronberg, Occurrence of Pharmaceuticals in River Water and Their Elimination in a Pilot-Scale Drinking Water Treatment Plant, Environ. Sci. Technol. 41 (2007) 5077–5084.
[6] E.M. Golet, A.C. Alder, W. Giger, Environmental Exposure and Risk Assessment of Fluoroquinolone Antibacterial Agents in Wastewater and River Water of the Glatt Valley Watershed, Switzerland, Environ. Sci. Technol. 36 (2002) 3645–3651.
[7] K.L. Jury, S.J. Khan, T. Vancov, R.M. Stuetz, N.J. Ashbolt, Are Sewage Treatment Plants Promoting Antibiotic Resistance? Crit. Rev. Environ. Sci. Technol. 41 (2011) 243–270.
[8] I. Ebert, J. Bachmann, U. Kühnen, A. Küster, C. Kussatz, D. Maletzki, C. Schlüter, Toxicity of the fluoroquinolone antibiotics enrofloxacin and ciprofloxacin to photoautotrophic aquatic organisms, Environ. Toxicol. Chem. 30 (2011) 2786–2792.
[9] V.S. Antonin, M.C. Santos, S. Garcia-Segura, E. Brillas, Electrochemical incineration of the antibiotic ciprofloxacin in sulfate medium and synthetic urine matrix, Water Res. 83 (2015) 31–41.
[10] L. Zhu, B. Santiago-Schübel, H. Xiao, H. Hollert, S. Kueppers, Electrochemical oxidation of fluoroquinolone antibiotics: Mechanism residual antibacterial activity and toxicity change, Water Res. 102 (2016) 52–62.
[11] M. Deborde, U. Von Gunten, Reactions of chlorine with inorganic and organic compounds during water treatment—Kinetics and mechanisms: A critical review, Water Res 42 (2008) 13–51.
[12] P. Wang, Y.-L. He, C.-H. Huang, Oxidation of fluoroquinolone antibiotics and structurally related amines by chlorine dioxide: Reaction kinetics product and pathway evaluation, Water Res. 44 (2010) 5989–5998.
[13] C.C. Kapałka, G. Fóti, C. Comninellis, Basic Principles of the Electrochemical Mineralization of Organic Pollutants for Wastewater Treatment, in: C. Comninellis, G. Chen (Eds.), Electrochemistry for the Environment, Springer, New York, 2010, pp. 1–21.
[14] H. Over, Surface chemistry of ruthenium dioxide in heterogeneous catalysis and electrocatalysis: from fundamental to applied research, Chem. Rev. 112 (2012) 3356–3426.
[15] A.J. Terezo, E.C. Pereira, Preparation and characterisation of Ti/RuO_2 anodes obtained by sol–gel and conventional routes, Mater. Lett. 53 (2002) 339–345.
[16] T. Razpotnik, J. Maček, Synthesis of nickel oxide/zirconia powders via a modified Pechini method, J. Eur. Ceram. Soc. 27 (2007) 1405–1410.
[17] J. Gaudet, A.C. Tavares, S. Trasatti, D. Guay, Physicochemical Characterization of Mixed RuO_2-SnO_2 Solid Solutions, Chem. Mater. 17 (2005) 1570–1579.
[18] X. Zeng, M. Zhang, X. Wang, X. Chen, X. Su, W. Tang, Effects of Sn content on Ti/RuO_2–SnO_2–TiO_2 anodes used in the generation of electrolyzed oxidizing water, J. Electroanal. Chem. 677–680 (2012) 133–138.
[19] J. Ribeiro, M.S. Moats, A.R. De Andrade, Morphological and electrochemical investigation of RuO_2–Ta_2O_5 oxide films prepared by the Pechini–Adams method, J. Appl. Electrochem. 38 (2008) 767–775.
[20] X. Wang, D. Tang, J. Zhou, Microstructure morphology and electrochemical property of RuO_2 70 SnO_2 30 mol % and RuO_2 30 SnO_2 70 mol % coatings, J. Alloys Compd. 430 (2007) 60–66.
[21] L.A. De Faria, J.F.C. Boodts, S. Trasatti, Electrocatalytic properties of Ru + Ti + Ce mixed oxide electrodes for the Cl_2 evolution reaction, Electrochim. Acta 42 (1997) 3525–3530.
[22] J. Wang, W. Zhu, X. He, S. Yang, Catalytic wet air oxidation of acetic acid over different ruthenium catalysts, Catal. Commun. 9 (2008) 2163–2167.
[23] H.E. Yun-nan, Z.H.U. Jun-qiu, Z. Teng, W. Xin, T. Dian, Effects of Composition on the Structure and Capacitive Properties of Ti/$(ZrO_2)_x(RuO_2)_{1-x}$ Electrodes, Chinese J. Struct. Chem. 32 (2013) 231–235.
[24] A.C. Bose, R. Ramamoorthy, S.N. Ramasamy, Nano-Metals I. Synthesis and Characterization of Nanocrystalline RuO_2-ZrO_2, Mater. Trans. 42 (2001) 1667–1671.
[25] J. Zhu, X. Wang, Z. Yi, Z. Tang, B. Wu, D. Tang, W. d Lin, Stability of Solid-Solution Phase and the Nature of Phase Separation in Ru–Zr–O Ternary Oxide, J. Phys. Chem. C 116 (2012) 25832–25839.
[26] X. Chen, G. Chen, Stable Ti/RuO_2-Sb_2O_5-SnO_2 electrodes for O_2 evolution, Electrochim. Acta 50 (2005) 4155–4159.
[27] X. Chen, G. Chen, P.L. Yue, Electrochemical Behavior of Novel Ti/IrOx-Sb_2O_5-SnO_2 Anodes Guohua, J. Phys. Chem. B 106 (2002) 4364–4369.
[28] R.E. Palma-Goyes, J. Vazquez-Arenas, R.A. Torres-Palma, C. Ostos, F. Ferraro, I. González, The abatement of indigo carmine using active chlorine electrogenerated on ternary Sb_2O_5-doped Ti/RuO_2-ZrO_2 anodes in a filter-press FM01-LC reactor, Electrochim. Acta 174 (2015) 735–744.

[29] F.A. Rodríguez, E.P. Rivero, L. Lartundo-Rojas, I. González, Preparation and characterization of Sb_2O_5-doped Ti/RuO_2-ZrO_2 for dye decolorization by means of active chlorine, J. Solid State Electrochem. 18 (2014) 3153–3162.
[30] R.E. Palma-Goyes, J. Vazquez-Arenas, C. Ostos, R.A. Torres-Palma, I. Gonzalez, The effect of ZrO_2 content on the microstructural and electro-catalytic properties of Sb_2O_5 doping Ti/RuO_2 anodes to yield active chlorine species, J. Electrochem. Soc. 163 (2016) H818–H825.
[31] M. Orazem, B. Tribollet, Electrochemistry, Electrochemical Impedance Spectroscopy, John Wiley & Sons, Inc., Hoboken, NJ, USA, 2008 Ch. 5.
[32] R.E. Palma-Goyes, J. Silva-Agredo, I. González, R.A. Torres-Palma, Comparative degradation of indigo carmine by electrochemical oxidation and advanced oxidation processes, Electrochim. Acta 140 (2014) 427–433.
[33] A.L. Giraldo, E.D. Erazo-Erazo, O.A. Flórez-Acosta, E.A. Serna-Galvis, R.A. Torres-Palma, Degradation of the antibiotic oxacillin in water by anodic oxidation with Ti/IrO_2 anodes: Evaluation of degradation routes organic by-products and effects of water matrix components, Chem. Eng. J. 279 (2015) 103–114.
[34] A.D. Becke, Perspective on Density functional thermochemistry. III. The role of exact exchange, Theoretical Chemistry Accounts, Springer Berlin Heidelberg, Berlin, Heidelberg, 2000, pp. 361–363.
[35] J. Tomasi, B. Mennucci, R. Cammi, Quantum Mechanical Continuum Solvation Models, Chem. Rev. 105 (2005) 2999–3094.
[36] R. Chen, V. Trieu, B. Schley, H. Natter, J. Kintrup, A. Bulan, R. Weber, R. Hempelmann, Anodic Electrocatalytic Coatings for Electrolytic Chlorine Production: A Review, Zeitschrift für Phys. Chemie 227 (2013) 651–666.
[37] M. Panizza, G. Cerisola, Direct And Mediated Anodic Oxidation of Organic Pollutants, Chem. Rev. 109 (2009) 6541–6569.
[38] W. Cheng, M. Yang, Y. Xie, Z. Fang, J. Nan, P.E. Tsang, Electrochemical degradation of the antibiotic metronidazole in aqueous solution by the Ti/SnO_2-Sb-Ce anode, Environ. Technol. 34 (2013) 2977–2987.
[39] C.A. Martinez-Huitle, S. Ferro, Electrochemical oxidation of organic pollutants for the wastewater treatment: direct and indirect processes, Chem. Soc. Rev. 35 (2006) 1324.
[40] C.A. Martínez-Huitle, E. Brillas, Decontamination of wastewaters containing synthetic organic dyes by electrochemical methods: A general review, Appl. Catal. B Environ. 87 (2009) 105–145.
[41] Y. Chen, S. Wang, X. Chen, Ti/RuO_2–Sb_2O_5–SnO_2 electrodes for chlorine evolution from seawater, Chem. Eng. J. 172 (2011) 47–51.
[42] P. Geng, J. Su, C. Miles, C. Comninellis, G. Chen, Highly-Ordered Magnéli Ti_4O_7 Nanotube Arrays as Effective Anodic Material for Electro-oxidation, Electrochim. Acta 153 (2015) 316–324.
[43] U. Neugebauer, A. Szeghalmi, M. Schmitt, W. Kiefer, J. Popp, U. Holzgrabe, Vibrational spectroscopic characterization of fluoroquinolones, Spectrochim. Acta Part A Mol. Biomol. Spectrosc. 61 (2005) 1505–1517.
[44] X. Van Doorslaer, K. Demeestere, P.M. Heynderickx, H. Van Langenhove, J. Dewulf, UV-A and UV-C induced photolytic and photocatalytic degradation of aqueous ciprofloxacin and moxifloxacin: Reaction kinetics and role of adsorption, Appl. Catal. B Environ. 101 (2011) 540–547.
[45] T. An, H. Yang, G. Li, W. Song, W.J. Cooper, X. Nie, Kinetics and mechanism of advanced oxidation processes (AOPs) in degradation of ciprofloxacin in water, Appl. Catal. B Environ. 94 (2010) 288–294.
[46] M.C. Dodd, A.D. Shah, U. Von Gunten, C.-H. Huang, Interactions of Fluoroquinolone Antibacterial Agents with Aqueous Chlorine: Reaction Kinetics Mechanisms, and Transformation Pathways, Environ. Sci. Technol. 39 (2005) 7065–7076.
[47] X. Xiao, X. Zeng, A.T. Lemley, Species-Dependent Degradation of Ciprofloxacin in a Membrane Anodic Fenton System, J. Agric. Food Chem. 58 (2010) 10169–10175.
[48] H. Ou, J. Ye, S. Ma, C. Wei, N. Gao, J. He, Degradation of ciprofloxacin by UV and UV/H_2O_2 via multiple-wavelength ultraviolet light-emitting diodes: Effectiveness intermediates and antibacterial activity, Chem. Eng. J. 289 (2016) 391–401.
[49] M.S. Yahya, N. Oturan, K. El Kacemi, M. El Karbane, C.T. Aravindakumar, M.A. Oturan, Oxidative degradation study on antimicrobial agent ciprofloxacin by electro-fenton process: Kinetics and oxidation products, Chemosphere 117 (2014) 447–454.